 CMES, vol.90, no.2, pp.165-177, 2013

A Hydrodynamic Assessment of a Remotely Operated Underwater Vehicle Based on Computational Fluid Dynamic – Part 1 – Numerical Simulation

Christian Boe, Jose Rodriguez, Carlos Plazaola, Ilka Banfield
Amaly Fong, Rony Caballero and Adan Vega

Abstract: The authors have developed a remote operate vehicle (ROV) that allow carried out highly risky task, in confined space such as inside of submerged sewers and pipes systems, areas were commercial ROV may not provide good performing. In addition, this ROV is low cost. This paper analyses based on the computational fluid dynamic the hydrodynamic performance of this ROV. The first part of the paper presents the theoretical approach and introduces the finite volume model developed in order to complete the study. Results of the model compare with published research shows good agreement. The second (forthcoming) part of the paper analyzes the hydrodynamic behavior of the ROV under different flow conditions.

Keywords: Remote Operated Vehicle, Confined Spaces, Hydrodynamic Behavior, Drag Forces, Computational Fluid Dynamic, Finite Volume Method.

1 Introduction

Divers usually perform maintenance task of underwater sewers and pipes systems. In some cases, the task to be carried out get so dangerous that divers live could be in danger, so the only option is the use of specially designed underwater vehicles. Although, commercial underwater vehicles has become popular, for some application, such as confined spaces and/or turbulent waters, they have not shown good results as they are not adequate neither are design for use in such environments (Choi, Yuh and Takashige (1995), Stone (2007) and Yuh (1990)).

Maneuver inside of a pipeline of small diameter is such a difficult task for the vehicle that the possibility of get crashed against the pipe wall, is largest that even the possibility of acquired good results from the task performed. This becomes an issue of interest from the point of view of engineering, more specifically, how to develop an underwater vehicle to perform maintenance task, such as survey, data

collection and so on inside pipes where unfavorable conditions, obstacles, water turbidity or impacts against the walls of the pipe can exists. The solution for above is to develop a special underwater vehicle with the ability to maneuver in confined spaces, such as inside narrow pipes, and also able to perform task usually only performed by extraordinarily high professional divers.

Remote Operate Vehicles (ROVs) are submersibles robots used in tasks related to maintenance, scientific research explorations and evaluation of submerged structures. Applications of ROV are increasing since new regions shall be explored every day. However, existing ROV presents some limitation, mainly because they cannot operate in every existing environment or are so expensive that only can be used in certain cases.

In order to develop a vehicle with such characteristics, many factors such as the shape, size, power, speed, configuration of the propellers, and others need to be thoroughly analyzed, since they affect the behavior of the ROV. Here is noteworthy to mention that performing such analysis is not an easy task. It is necessary to utilize tools that help us to find out unknown responses otherwise, the final product to be design will probably result in loss of time and money, been the computational fluid dynamic (CFD) the best ally in achieving this goal.

CFD has been gaining so many adepts since the computer capacity has increased, together with the decrease on the prices, and the increasing number of commercial codes appearing in the last decades. Nowadays, the usage of CFD is almost a necessity in various fields of the engineering science (Gardano and Dabnichki (2006), Ozaki, Hashiguchi, Okayasu and Chen (2007), Avila, Han, and Atluri (2011)). Applications of CFD for the study of the hydrodynamic behavior of ROV exist (Rhee and Joshi (2005), Valencia (2008), Kulczyk, Skraburski and Zawislak (2007), Husaini, Samad and Arshad (2011)) however, still many tasks to be done before we can say that CFD is the replacement of hydrodynamic experiments.

In this paper, a numerical analysis is perform in order to study the hydrodynamic behavior of an ROV specially designed for maintenance task, such as inspection, data, video and photo collection in confined spaced. Using different software of computational fluid dynamics, such as ANSYS FLUENT, ANSYS CFX and STAR-CCM, simulations were performed. The study has two parts, due to its extension. The first one is within this report; the second part will be publishing separately. The mathematical principles as well the finite volume model and its validation is discusses here. Comparison with experiment of other ROV that presents certain levels of similarity is also presented. Sensitive analysis of hydrodynamic behavior of the ROV under different flow condition is presented in the second part of the paper.

2 General view of the ROV for confined spaces inspection

The hydrodynamic behavior of an underwater vehicle is essentially due to the non-linear nature of the rigid body. With various degrees of freedom and subjected to hydrodynamic forces, which are not always easy to determine, the ROV become in an interesting field of study (Valencia (2008)). Figure 1 shows the image of the ROV. The nomenclature used is based on SNAME (Society of Naval and Marine Engineers). This notation is use to describe the marine vehicle movement as seen in Table 1 (SNAME, 2010). As seen the ROV has a spherical body composed of two main parts, both of them are essentially discs that allow incorporates all the electronic elements inside the discs and cameras and illumination system outside. It has eight propellers strategically located in order to perform any moving needed without the risk of losing them due to impacts or flooding.

The total diameter of the vehicle is about 60 cm and it weight about thirty kilograms including all the components. It is design to operate inside pipes with a diameter larger than one (1) meter and not deeper than hundred (100) meters. The main body of the ROV is built of aluminum alloys, and its design allows withstand moderate impacts against pipe walls.

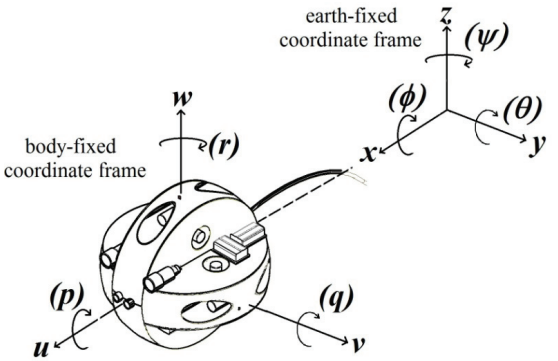

Figure 1: ROV fixed-body reference frame

3 Prediction of the hydrodynamic behavior of the ROV

The analysis focused on the Eulerian description approach which allows seeing the connection between the dynamics derivatives in a ground reference frame and a fixed body reference frame, which it is crucial in order to study the hydrodynamic behavior of the ROV. The equation describing the motion of the vehicle consists

Table 1: Notation for marine vehicles SNAME

Movement	Position and orientation	Linear and angular velocity
Surge	x	u
Sway	y	v
Heave	z	w
Roll	f	p
Pitch	q	q
Yaw	y	r

of a nonlinear differential matrix equation as shown in Equation 1 (Chin and Lau (2012)).

$$\mathbf{M}\dot{\nu} + \mathbf{C}(\nu)\nu + \mathbf{D}(\nu)\nu + \mathbf{g}(\eta) = \boldsymbol{\tau} \tag{1}$$

Where, **M** is the sum of the inertia matrix of the rigid body and the inertia matrix of the additional fluid. The matrix M can be described as shown in Equation 2. (Wang and Clark (2007)).

$$\mathbf{M} = \begin{bmatrix} m+X_{\dot{u}} & 0 & 0 & 0 & mz_G & -my_G & 0 & -mz_G \\ 0 & m+Y_{\dot{v}} & 0 & -mz_G & 0 & mx_G & mz_G & 0 \\ 0 & 0 & m+Z_{\dot{w}} & my_G & -mx_G & 0 & -my_G & mx_G \\ & & & my_G & I_{xx}+K_{\dot{p}} & 0 & 0 & \\ & & & -mx_G & 0 & I_{yy}+M_{\dot{q}} & 0 & \\ & & & 0 & 0 & 0 & I_{zz}+N_{\dot{r}} & \end{bmatrix} \tag{2}$$

C is the sum of the forces due to the Coriolis forces and moments, and the cen-

tripetal additional mass as is shown in Equation 3.

$$C = \begin{bmatrix} 0 & 0 & 0 \\ 0 & 0 & 0 \\ 0 & 0 & 0 \\ -m(y_G q + z_G r) & m(y_G p + w) - Z_{\dot{w}} w & m(z_G p - v) + Y_{\dot{v}} v \\ m(x_G q - w) + Z_{\dot{w}} w & -m(z_G r + x_G p) & m(z_G q + u) - X_{\dot{u}} u \\ m(x_G r + v) - Y_{\dot{v}} v & m(y_G r - u) + X_{\dot{u}} u & -m(x_G p + y_G q) \end{bmatrix}$$
$$\begin{bmatrix} m(y_G q + z_G r) & -m(x_G p - w) - Z_{\dot{w}} w & -m(x_G r + v) - Y_{\dot{v}} v \\ -m(x_G q - w) + Z_{\dot{w}} w & m(z_G r + x_G p) & -m(y_G r - u) - X_{\dot{u}} u \\ -m(x_G r - v) - Y_{\dot{v}} v & -m(z_G q + u) + X_{\dot{u}} u & m(x_G p + y_G q) \\ 0 & I_{zz} q - N_{\dot{r}} r & -I_{yy} p + M_{\dot{q}} q \\ -I_{zz} q + N_{\dot{r}} r & 0 & m(z_G q + u) - X_{\dot{u}} u \\ I_{yy} q - M_{\dot{q}} q & m(y_G r - u) + X_{\dot{u}} u & 0 \end{bmatrix} \quad (3)$$

D is the damping matrix due to the fluid surrounding the vehicle given by equation 4.

$$\mathbf{D} = \begin{bmatrix} X_u & 0 & 0 & 0 & 0 & 0 \\ 0 & Y_v & 0 & 0 & 0 & 0 \\ 0 & 0 & Z_w & 0 & 0 & 0 \\ 0 & 0 & 0 & K_p & 0 & 0 \\ 0 & 0 & 0 & 0 & M_q & 0 \\ 0 & 0 & 0 & 0 & 0 & N_r \end{bmatrix} \quad (4)$$

The array of forces and moments **g** are due to the weight and buoyancy, transformed to a reference frame fixed to the vehicle and given by Equation 5.

$$g(\eta) = \begin{bmatrix} (W - B)\sin(\theta) \\ -(W - B)\cos(\theta)\sin\phi \\ -(W - B)\cos\theta\cos\phi \\ y_B B\cos\theta\cos\phi - z_B B\cos\theta\sin\phi \\ -z_B B\sin\theta - x_B B\cos\theta\cos\phi \\ x_B B\cos\theta\sin\phi + y_B B\sin\theta \end{bmatrix} \quad (5)$$

Finally, $\boldsymbol{\tau}$ is the input vector of forces and moments. It relates to the output vector of the thrust, to the matrix configuration of the thrusters, to the dynamics of individual thrusters as well as to the conversions of the input signals to the drive voltage of the vehicle drivers as shown in Equation 6.

$$\boldsymbol{\tau} = \mathbf{T}u \quad (6)$$

This paper analyzes the behavior of the vehicle to move in the direction $\widehat{\mathbf{x}}$. Therefore, determining the component $\boldsymbol{X}_u$ of the damping matrix is the first goal. Others movements of the vehicle will be studied in the second part of the paper. To achieve this, parametric study is perform with the aid of computational fluid dynamics.

4 Method of Analysis

To carry out this study, computational fluid dynamic was used. ANSYS FLUENT, ANSYS CFX and STAR-CCM software were utilized for the simulation. The turbulence model called k-w (a Reynold Averaged Navier-Stoke based turbulence model) was used to simulate the parameters. The information is collected for each case and analyzed in a post-processor which organizes, graphics and animated simulation data.

4.1 Model development

The mechanical model has several small appendages, propellers and a trailing tether line as can be seen in Figure 1. These objects were not considered in the model. In addition to above, the design was lightly changes to have a smoother surface. With this smooth surface the hull could be cut out of a sphere, the radius becoming slightly larger than the original design at 0.3 meters.

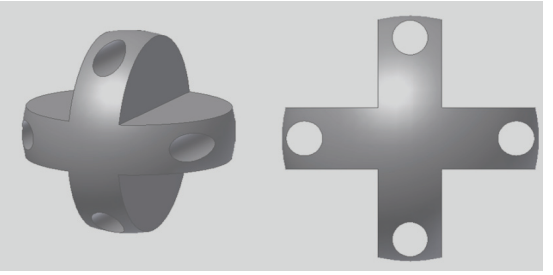

Figure 2: Simplified 3D representation of the ROV

4.1.1 Mesh Generation

STAR-CCM, CFX and ANSYS Fluent has its own meshing approach that was used. A structured mesh was created containing two volumetric controls. The purpose of the first volumetric control is to improve the mesh around the ROV model, and wake zone. The purpose of the following volumetric control was to create a transitioning phase between the first volumetric control and the base mesh size, to avoid volume aspect ratios becoming too large. Another purpose was to capture the wake region.

The characteristics of the volumetric controls are shows in Table 2. Near surfaces and wake regions, more details needed to be captured, and would require a finer mesh.

A custom mesh element size was also chosen for the surfaces of the ROV. The finest mesh is required near the surfaces of the ROV.

Table 2: Characteristics of the volumetric controls.

Volumetric Control	Size [m]	Mesh size [mm]
1	-.08x2.8x0.8	30
2	-1.8x3.6x1.8	100

After several changes to the ROV surface mesh size and volumetric controls, the final solution had 1.55 million mesh elements.

4.1.2 Boundary Condition

The ROV will operate fully submerged as the environments it will navigate would initially be lock chambers, pipes and culverts. A culvert was chosen as a domain. Thus, the boundaries would be the culvert wall, an inlet and an outlet. The diameter of the model would be large enough to avoid the Venturi effect. Avoiding any sources of inaccuracies in the calculation is essential, and pressure is presumed to be the largest part of the drag force.

A turbulent flow in a pipeline would eventually develop a velocity profile if the pipe is of sufficient length. The length required for this, for any of the velocities, would be far too long to compute. The final length chose would not try to capture this effect, but rather the wake of the ROV which is essential to the drag force.

The hydrodynamic effect of the no slip condition is crucial to determining the drag force of the ROV. There are several ways to approach this problem when creating the mesh. The Prism Layer function was activated and customized. Five prism layers were applied as seen in Figure 5, and this proved a good solution. Prism layers were not applied to the surface of the culvert wall because the simulation time would have increased, and the wall is of no importance. In the case of the ROV the prism layer near the surface is show in Figure 3.

4.1.3 Initial working condition

The ROV is designed to examine objects in confined spaces with dark murky water. Large sub-sea offshore ROVs will reach speeds of 2-5 knots. However, the conceptual ROV will not have the need to move at this speed. Three velocities

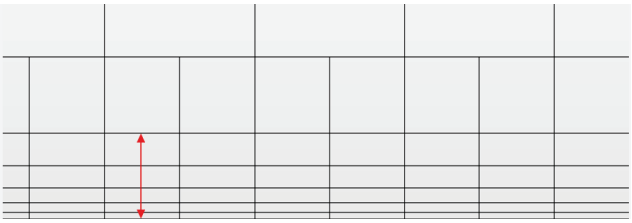

Figure 3: Prism layers near to the surface of the ROV

in between the operation range of the vehicle were chosen for the simulations as shown in Table 3.

In the lock chamber, the ROV can reach max speed to reach its destination. The area will be open with no obstacles to avoid. Inside the culvert, maximum speed will not be recommended as the water will be extremely dark and murky. Objects to avoid might suddenly appear and will have to be avoided. When performing inspections the velocity should be very small so that images can be captured properly without any interference. The Reynolds number of the three simulations is shown in Table 4.

It is presumed that the ROV will share many hydrodynamic characteristics with a sphere. The high Re numbers will imply that the nature of the flow will be turbulent, according to (Jones and Clarke (2008)).

Table 3: Data of velocities used in the analysis

Velocity [m/s]	Operation area	Purpose
0,5	Lock chamber	Max velocity
0,2	Culvert	Cruise velocity
0,05	Culvert/pipe	Inspection velocity

Table 4: Reynold number of the simulations

Variable	Values	Velocity [m/s]	Reynolds number
ρ [kg/m^3]	1000	0,05	3,76E+04
μ [N s/m^2]	7,98E-04	0,2	1,50E+05
L [m]	0,6	0,5	3,76E+05

4.1.4 Turbulence model for the simulations

The purpose of these simulations is to determine the drag forces of the ROV. The main factors of this are the pressure and velocity attributes surrounding the ROV. The K-ω model can simulate situations with high pressure gradients exceptionally well. K-ω was chosen it over the K-ε model, due to the poor predictions of the K-ε in regards to flow separation under high pressure gradients. A factor the K- ω has predicted much better according to Atkins (2002).

The K- ω model is a Reynolds Averaged Navier-Stokes based turbulence model. It is a two-part equation model, with one equation for solving the turbulent kinetic energy k. The other equation solves the dissipation rate ω. Additionally there is the Menter Shear Stress Transport K-ω model that further improves the standard K-ω model by incorporating some aspects of the K- ε to improve the K-ω near the wall, where it is weak (CD-adapco (2012)).

The hydrodynamic forces involved in the problem are the drag and lift forces. Since no part of the vehicle has geometry similar to a wing profile, including the rings do not have this form, the lift forces are negligible in comparison to the forces due to the drag.

Equation 7 shows the mathematical model used to obtain the vehicle drive force to different input conditions.

$$\overrightarrow{D} + \overrightarrow{L} = \int_{S_b} p.d\overrightarrow{S} + \int_{S_b} \overline{\overline{\tau}}.d\overrightarrow{S} \tag{7}$$

The first term on the right is the component determining the forces due to the pressure exerted by the fluid on motion of the carrier surface, and the second term of the right side of the equation indicates the forces due to viscous stresses, which is equivalent to the rate of deformation.

Thus, the pulling force in the direction of movement of the vehicle occurs by means of the Equation 8.

$$F_D = \int_s p \cos\theta \; d\overrightarrow{S} + \int_s \overline{\overline{\tau}} \sin\theta d\overrightarrow{S} \tag{8}$$

Where F_D is the drag force, **p** is the fluid pressure acting on the surface of the body, $\boldsymbol{\theta}$ is the angle of the surface relative to the direction of the flow velocity towards the vehicle, $\overline{\overline{\boldsymbol{\tau}}}$ is viscous shear stress and **S** is surface area. Thus, the drag force is the force parallel to the direction of flow velocity of a fluid as is given by Equation 9.

$$C_D = 2F_D/\rho A v^2 \tag{9}$$

The components of the drag force are constituted by the effects of pressure. This component can be call drag by pressure, and cause by the shear viscous stresses can be called frictional drag. Both types of drag occur simultaneously, but the force due to friction drag plates often occurs in vehicles with thin cross sections, which is not the case in the ROV designed.

5 Analysis Procedure

The simulations were divided into three stages. The first stage was a steady-state simulation. With this steady state solution, the unsteady simulation would have a motive to work upon as it is demonstrated in Jones and Clarke (2008). The second stage was to simulate the first second of movement accurately. This would make the rest of the simulation a good reason to work. The final stage simulated the flow for ten seconds. Each stage was almost 1000 iterations. See table 5.

Results are compared to experimental and empirical data from hydrodynamic assessments of spheres. The ROV 3D model was originally a sphere then the features were extruded. This provides a good foundation for a geometric comparison.

The force distribution of the ROV has less viscous forces than a sphere. Though the ROV has a slightly larger surface area the velocity profile is much different. The high velocity areas, on the outer edges of the ballast tanks, are much smaller than a sphere, due to the thruster tunnels preventing the flow from continually accelerating towards the outer edges. The flow separation following the leading edges of the ballast tanks causes the velocity to decrease. Thus, much of the surface area of the ROV has provided no viscous forces.

The cross section of the ROV is much smaller than a sphere, though the surface areas are almost identical as shown in Table 6.

The drag coefficient curve can be divided into 10 segments. These segments can be used to calculate the drag coefficient of a sphere depending only on the Reynolds number. See table 7.

6 Analysis of the results

A quick calculated comparison between the formulae in table 7 with the experimental drag coefficient values of Jones and Clarke (2008) proved them to be accurate. Table 8 lists the values to be compared. The sphere drag forces are larger than the ROV drag forces. This can be explained by comparing the cross sections and wake patterns. The difference between cross sections of the objects is ROV/Sphere = 47% calculated from table 6. Pressure forces depend on this and contribute to 90% of the drag force. Therefore, it could be presumed that the ROV forces could be 47% that of a sphere.

Table 5: Simulation Structure

			Iterations	Time Steps	
Stage	State	Time [s]	Total	Amount	Size [s]
1	Steady		900		
2	Unsteady	1	900	30	0,03
3	Unsteady	1-15	900	45	0,33
	Total	15	2700	75	

Table 6: Geometric information of the ROV model and a sphere

Comparison	Cross section [m^2]	Surface area [m^2]
Sphere	0,283	1,131
ROV	0,133	1,145

Table 7: Segmented formulae for the sphere drag coefficient

For $1.2 \times 10^4 \leq Re \leq 4.4 \times 10^4$	$log_{10}C_D = -1.9181 + 0.6370w - 0.0636w^2$
For $4.410^4 \leq Re \leq 3.8 \times 10^5$	$log_{10}C_D = -4.3390 + 1.5809w - 0.1546w^2$
For $3.8 \times 10^5 \leq Re \leq 4 \times 10^5$	$C_D = 29.78 - 5.3w$
For $4 \times 10^5 \leq Re \leq 10^6$	$C_D = 0.1w - 0.49$

Table 8: Results compared to calculated sphere data

		Force		Coefficient		
Speed	Re	ROV	Sphere	ROV	Sphere	ROV/Sphere Force
0,05	3,7E4	0,068	0,1602	0,409	0,4534	42 %
0,2	1,5E5	1,015	2,8460	0,381	0,5033	36 %
0,5	3,7E5	6,321	8,1818	0,380	0,2315	77 %

7 Conclusions

With the simulation structure built, three separate simulations were executed with different velocities. The purpose of three simulations was to simulate different operation profiles. With several simulations, a drag coefficient could additionally be proven. After complete the first part of this paper the following conclusions are drawn.

1. The hydrodynamic design of the ROV is proven to be carefully designed with a low drag coefficient of 0.38 as seen in Table 8.

2. There will be an increase of drag considering the missing appendages, such as thrusters, lighting and optical devices and the tether cable.

3. The drag forces are small enough to be manageable by the thrusters. The maximum speed could be increased beyond 0.5 m/s.

Acknowledgement: The authors wish to thank to the National Secretary of Science and Technology of Panama (SENACYT) and Class IBS for their support during this research project.

References

Atkins, W. S. (2002): NSC Best Practice Guidelines for Marine Applications of CFD.

Chin C.; Lau M. (2012): Modeling and Testing of Hydrodynamic Damping Model for a Complex-shaped Remotely-operated Vehicle for Control. *J. Marine Sci. Appl.* 11: 150-163.

Choi, S.K.; Yuh, J.; Takashige, G.Y. (1995): Development of the Omni Directional Intelligent Navigator. *Robotics & Automation Magazine*, IEEE.

CD-adapco (2012): STAR-CCM+ User Manual.

Husaini, M.; Samad Z.; Rizal Arshad M. (2011): Autonomous Underwater Vehicle Propeller Simulation using Computational Fluid Dynamics. *Journal of Computational Fluid Dynamic Technologies and Applications*. 294-314.

Jones, D.A; Clarke, D.B. (2008): Simulation of Flow Past a Sphere using the Fluent Code. *Defense Science and Technology Organization*. Australia.

Kulczyk, J.; Skraburski L.; Zawislak M. (2007): Analysis of screw propeller 4119 using the Fluent system, Worclaw University of Technology.

Ozaki S.; Hashiguchi K.; Okayasu T.; Chen D.H. (2007): Finite Element Analysis of Particle Assembly-water Coupled Frictional Contact Problem. *CMES: Computer Modeling in Engineering & Sciences*, Vol. 18, No. 2, pp. 101-120.

Paola Gardano; Peter Dabnichki (2006): Application of Boundary Element Method to Modelling of Added Mass and Its Effect on Hydrodynamic Forces. *CMES: Computer Modeling in Engineering & Sciences*, Vol. 15, No. 2, pp. 87-98.

Rhee S.; Joshi S. (2005): Computational validation for flow around a marine propeller using unstructured mesh based Navier-stokes solver. *JSME International Journal*, 48(3).

Ruben Avila; Zhidong Han; Satya N. Atluri (2011): A novel MLPG-Finite-Volume Mixed Method for Analyzing Stokesian Flows & Study of a new Vortex Mixing Flow. *CMES: Computer Modeling in Engineering & Sciences*, Vol. 71, No. 4, pp. 363-396.

SNAME (2010): Publication of The Society of Naval Architects & Marine Engineers.

Stone W. (2007): Design and Deployment of a 3D Autonomous Subterranean Submarine Exploration Vehicle. Stone Aeroespace / PSC, Inc.

Valencia R. (2008): Fluid and structural simulation of a ROV. Universidad EAFIT, Medellin – Colombian.

Wang W.; Clark C. M. (2007): Autonomous Control for a Differential Thrust ROV. Proceedings of the 2007 International Symposium on Unmanned Untethered Submersible Technology.

Yuh J. (1990): Modeling and Control of Underwater Robotic Vehicles. *IEE Transactions on Systems, Man and Cybernetics*, vol. 20. No. 6.